Tanaka, Y., Klemann, V., Okuno, J. (2009): Application of a Numerical Inverse Laplace Integration Method to Surface Loading on a Viscoelastic Compressible Earth Model. - Pure and Applied Geophysics, 166, 8-9, 1199-1216

DOI: 10.1007/s00024-009-0508-y

Application of a Numerical Inverse Laplace Integration Method to Surface Loading in a Viscoelastic Compressible Earth Model

Y. Tanaka

Geodetic Department, Geographical Survey Institute, Ibaraki, Japan

(present address: Earthquake Research Institute, The University of Tokyo, Tokyo, Japan)

V. Klemann

Department 1, Geodesy and Remote Sensing, GeoForschungsZentrum Potsdam, Potsdam, Germany

J. Okuno

Earthquake Research Institute, The University of Tokyo, Tokyo, Japan

Normal mode approaches for calculating viscoelastic responses of self-gravitating and compressible spherical earth models have an intrinsic problem of determining the roots of the secular equation and the associated residues in the Laplace domain. To by-pass this problem, a method based on numerical inverse Laplace integration was developed by Tanaka et al. [2006, 2007] for computations of viscoelastic deformation caused by an internal dislocation. The advantage of this approach is that the root-finding problem is avoided without imposing any additional constraints on the governing equations and earth models. In this study, we apply the same algorithm to computations of viscoelastic responses to a surface load, and show that results obtained by this approach agree well with those obtained by a time-domain approach that

---

Y. Tanaka, Geodetic Department, Geographical Survey Institute of Japan, 1, Kitasato, Tsukuba, Ibaraki, 305-0811, Japan. (ytanaka@gsi.go.jp, fax: +81-298-64-1802), present address: Earthquake Research Institute, The University of Tokyo, 1-1-1, Yayoi, Bunkyo-ku, Tokyo, 113-0032, Japan. (y-tanaka@eri.u-tokyo.ac.jp, fax: +81-3-5841-)

V. Klemann, Department 1, Geodesy and Remote Sensing, GeoForschungsZentrum Potsdam, Telegrafenberg, D-14473 Potsdam, Germany. (volkerk@gfz-potsdam.de)

J. Okuno, Earthquake Research Institute, The University of Tokyo, Bunkyo-ku, Tokyo, 113-0032, Japan. (okuno@eri.u-tokyo.ac.jp)

does not need determinations of the normal modes in the Laplace domain. Using an elastic earth model PREM and a convex viscosity profile, we calculate viscoelastic load Love numbers (h, l, k) for compressible and incompressible models. Comparisons between the results show that effects due to compressibility are consistent with results obtained by previous studies, and the rate differences between the two models can amount to 10-40%. This method will serve as an independent method to confirm results by time-domain approaches, and will be useful to increase reliability for modeling postglacial rebound.

1. Introduction

Peltier [1974]'s normal-mode method provided us with the basic framework in theoretical studies of postglacial rebound assuming viscoelasticity of the earth mantle [e.g. Wu and Peltier, 1982]. It has, however, been known that the classical normal mode approach has suffered from the intrinsic difficulties which arise when compressibility and self-gravitation are considered simultaneously in the governing equations [Wu and Peltier, 1982; Wolf, 1985b; Han and Wahr, 1995; Plag and Jüttner, 1995; Vermeersen et al., 1996]. To circumvent these difficulties, initial value approaches in the time-domain [e.g. Hanyk et al., 1995] have been used. In this paper, after a short review of previous studies, we introduce an alternative method to compute surface loading of spherically symmetric, self-gravitating and compressible earth models with continuously varying viscoelastic profiles by applying a numerical inverse Laplace integration method developed for computations of global post-seismic deformation [Tanaka et al., 2006, 2007]. Moreover, we investigate the influence of compressibility for a finely layered earth model.

2. The intrinsic numerical difficulties

2.1. The root finding problem

In the normal mode theory, the governing equations (quasi-static equation of motion, equation of continuity and Poisson's equation [e.g. Dahlen, 1974] and a viscoelastic constitutive equation [e.g. Peltier, 1974]) are transformed into those for the corresponding elastic medium in the Laplace domain, and inverse relaxation times and associated relaxation modes are determined by solving the characteristic equation numerically [e.g. Wu and Peltier, 1982]. In contrast to incompressible models, where the solutions are represented by a sum of discrete relaxation modes [Wu and Peltier, 1982; Wolf, 1985a; Wu and Ni, 1996; Boschi et al., 1999], a denumerably infinite number of modes (= dilatation modes [Vermeersen et al., 1996]) exists in the presence of compressibility and self-gravitation. The numerical root finding algorithms do not work for identifying these roots associated with dilatation modes [Han and Wahr, 1995]. (In addition, a difficult identification of roots can be observed also for incompressible models that include a viscoelastic lithosphere [Spada and Boschi, 2006].)

2.2. The instability modes

In addition to the root finding problem, if the density and the elastic structure in the earth models does not satisfy the Adams-Williamson equation [Bullen, 1975], unstable modes with positive relaxation times appear [Plag and Jüttner, 1995]. The elastic earth model PREM [Dziewonski and Anderson, 1981] is not consistent with this relation, since there are density inversions in the upper mantle with depths shallower than 220 km, which cause Rayleigh-Taylor instabilities [Plag and Jüttner, 1995]. Hanyk et al. [1999] found that the characteristic times of unstable modes for earth models with a few number of discrete layers are on the order of ten thousand years and cannot be neglected in applications to postglacial rebound. Vermeersen and Mitrovica [2000] later showed that the characteristic times of unstable modes become much longer for finely layered earth models, such as PREM, with relatively smaller density contrasts at internal boundaries and their contributions are negligible on geological time scales. Most likely, these density inversions do not occur in the real Earth on larger time scales, as convective motions would wipe them out. Further details on this can be found at the end of the introduction in Vermeersen and Mitrovica [2000].

3. Previous methods

In order to by-pass the above two difficulties, several methods have been proposed. A first approach is to modify the governing equations and to express compressibility and self-gravitation approximately [Wolf, 1985b, 1997; Purcell, 1998; Wolf and Kaufmann, 2000; Martinec et al., 2001; Wolf and Li, 2002; Klemann et al., 2003]. A detailed classification for the various incremental field equations and their physical meanings can be found in Wolf [1997] and Klemann et al. [2003]. Using these formulations, dilatation modes and unstable modes vanish and consequently one can obtain closed-form solutions.

A second approach is an approximate evaluation of dilatation modes without modifying the governing equations. Vermeersen et al. [1996] devised an approximate formula, which was later corrected by Hanyk et al. [1999] to find the roots of the dilatation modes in homogeneous and two-layer earth models. This method, however, has not been applied to finely layered earth models.

A third possibility are numerical approaches, which include those based on the Laplace transformation and those implemented in the time-domain. For incompressible models, both have been developed [e.g. Fang and Hager, 1994, 1995; Martinec, 2000; Zhong et al., 2003; Spada and Boschi, 2006]. For compressible models, only time-domain approaches [e.g. Hanyk et al., 1995; Steffen et al., 2006] have been used. Since the governing equations are solved in the time domain, effects of all modes including dilatation modes are evaluated without finding the roots.

Therefore, for *compressible and finely stratified* earth models, only time-domain approaches have been employed without imposing additional constraints.

4. Proposed method

4.1. Governing equations and load Love numbers

The equations of equilibrium for a self-gravitating, spherically symmetric and compressible sphere initially in hydrostatic equilibrium can be reduced to a set of ordinary differential equations of first order in the Laplace domain [e.g. Wu and Peltier, 1982]:

$$\frac{d\tilde{\mathbf{y}}_n(r;s)}{dr} = \tilde{\mathbf{A}}_n(r;s)\tilde{\mathbf{y}}_n(r;s) \tag{1}$$

where r is the radial distance and $\tilde{\mathbf{y}}_n(r;s)$ the radial functions associated with displacement, stress and gravity potential of the spheroidal mode. n, s and the tilde represent the spherical harmonic degree, the Laplace variable and Laplace transform, respectively. Viscoelasticity is considered in Eq. (1), and the coefficient matrix $\tilde{\mathbf{A}}_n(r;s)$ for a Maxwell rheology is explicitly given in Wu and Peltier [1982]. Integrating Eq. (1) with the boundary conditions appropriate for surface load [Wu and Peltier, 1982] applying the Runge-Kutta-Gill method [e.g. Press et al., 1992], we obtain load love numbers $((\tilde{h}_n, \tilde{l}_n, \tilde{k}_n)(s))$ corresponding to the vertical and horizontal displacements and the gravity potential change at the surface in the Laplace domain [Wu and Peltier, 1982]. Then, the load Love numbers in the time domain are

$$(h_n, l_n, k_n)(t) = \frac{1}{2\pi i}\int_{c-i\infty}^{c+i\infty} (\tilde{h}_n, \tilde{l}_n, \tilde{k}_n)(s)\frac{e^{st}}{s}ds \tag{2}$$

where s in the denominator shows that Heaviside loading is applied and a Bromwich path is assumed, and c is a real constant larger than the largest root.

4.2. Numerical inverse Laplace transformation

In order to evaluate the Laplace inversion, we can replace the integration path in Eq. (2) by a rectangular path around the real axis of s, since the roots of the secular equation are real numbers [Tanaka et al., 2006]. A root finding algorithm is used only for searching for the largest and smallest roots. By setting an appropriate path enclosing these two roots, contributions from all roots, including those of the dilatation modes and positive roots, are calculated simultaneously [Tanaka et al., 2006]. This method was already applied in Tanaka et al. [2006] in order to solve Eq. (1) for another set of boundary conditions, namely an internal dislocation and the free surface. The numerical Laplace integration is carried out with the Romberg integration method combined with ordinary polynomial interpolation [Press et al., 1992]. The integrands are continuous and vary smoothly along the employed path, and the principal branch for the elastic response at $t = 0$ agrees with the result obtained by an independent method [Tanaka et al., 2006, 2007]. The stability of the integration and the detailed process to determine the integration path are described in these papers.

For the earth model based on the PREM that we use in the following, positive roots tending to instability exist. Their consideration causes negligible errors in estimating viscoelastic responses up to time scales shorter than a few million years on which the linearized viscoelastic theory holds [Plag and Jüttner, 1995; Vermeersen and Mitrovica, 2000]. Excluding these modes from the integration path would lead to discrepancies in the elastic deformation if compared to results computed with theory of elastic deformation, since in our model the upper mantle density inversions are retained also for elastic calculations.

To validate our method, we compare the viscoelastic load Love numbers obtained by this method with results published in previous studies. Figure 1 (top) displays a comparison with results by Hanyk et al. [1995] for a continuously varying viscosity profile (Eq. (9) in their paper) in conjunction with the PREM. We see that both viscoelastic responses agree well with each other. In order to compute responses for an incompressible earth model, the Lamé's constant λ is set to a large value ($= 100\mu$) without setting up the differential equation system for the incompressible case [Wu and Peltier, 1982]. Figure 1 (bottom) shows a good agreement between the result for the 200-layer PREM model of Spada and Boschi [2006] and that for the same model obtained by the presented approach.

5. Effects of compressibility

Taking into account effects due to compressibility in viscoelastic modeling is important not only regarding theoretical aspects but also for geophysical applications. Vermeersen et al. [1996] showed that differences between true polar wander computed with a compressible two-layer model and that computed with the corresponding incompressible one can amount to 30%. The formulations based on incompressibility [Wolf and Li, 2002], on the other hand, give an excellent approximation to the compressible response near the long times. However, differences in the shorter-term response have not been examined yet. In this section, we calculate differences between compressible and incompressible models and investigate if major effects due to compressibility are seen in a finely layered model including a lithosphere.

5.1. Earth model

We employ PREM with liquid outer and solid inner core. The viscosity is 10^{40} Pa s down to the depth of 120 km, which accounts for the elastic lithosphere. The viscosity in the mantle (3480 km $< r <$ 6251 km) is shown in Figure 2, which is obtained by a polynomial interpolation of the convex viscosity profile [Ricard and Wuming, 1991] used in previous studies [e.g. Hanyk et al., 1995; Vermeersen and Sabadini, 1997; Spada and Boschi, 2006]. In the solid core, the viscosity is 10^{25} Pa s, which effectively behaves as an elastic body.

The physical process of surface loading is governed by the flexural rigidity, rather than the elastic rigidity [Turcotte and Schubert, 1982]. To correctly consider effects due to compressibility on surface loading, we construct the corresponding incompressible model by replacing the elastic rigidity in the above model $\mu_{cmp}(r)$ by $\mu_{inc}(r) = 0.5\mu_{cmp}/(1-\nu_{cmp})$, which satisfies the following scaling law associated with the flexural rigidity, D_e [Lambeck and Nakiboglu, 1980]:

$$\frac{dD_e}{dr} = \frac{2\mu_{cmp}(r)L^2}{1-\nu_{cmp}(r)} = \frac{2\mu_{inc}(r)L^2}{1-\nu_{inc}(r)}, \tag{3}$$

where $\nu_{cmp}(r) = \frac{\lambda_{cmp}(r)}{2(\lambda_{cmp}(r)+\mu_{cmp}(r))}$ is the Poisson's ratio, $\nu_{inc}(r) = \frac{100\mu}{2(100\mu+\mu)} \simeq 0.5$, and L is the lithospheric thickness. In the incompressible model of Vermeersen et al. [1996], the elastic rigidity is the same as for the compressible model, since the flexural rigidity cannot be defined for the two-layer core-mantle model excluding a lithosphere.

5.2. Comparison in load Love numbers

5.2.1. Love number *h*

Figure 3 (a) displays the computed viscoelastic load Love numbers $h_n^{cmp}(t)$ for the compressible and $h_n^{inc}(t)$ for the incompressible models for selected harmonic degrees. First, we examine differences between $h_n^{cmp}(t)$ and $h_n^{inc}(t)$ at $t = 0.1$ kyr which approximates the elastic limit. The signature of h_n is negative for both models, indicating that subsidence occurs in the vicinity of the applied load. For $n \leq 10$, the vertical deformation is larger for the compressible model, and the differences decrease with n (30% for $n = 2$ and 5% for $n = 10$). This agrees with the previous result that compressibility enhances the elastic deformation [Wolf, 1985b; Vermeersen et al., 1996], although we already assumed a reduced shear modulus for the incompressible model. For $n \geq 25$, however, the vertical deformation is larger for the incompressible model, and the differences increase with n (up to 10% for $n = 150$). This results from the different definition of the incompressible model, since the initial deformation for the compressible model is larger for all the degrees, when we use the incompressible model with the same elastic rigidity as the compressible model (Figure 3 (b)). We also note from the figure that by using the incompressible model satisfying the scaling law, the differences between the incompressible and compressible models become smaller. Next, the vertical deformation at $t = 1,000$ kyrs is larger for the compressible model up to degree 25, but becomes smaller for higher degrees. The relative difference in the vertical deformation between t=0.1 and 1,000 kyr is the largest for $n = 70$.

To discuss effects due to compressibility on vertical deformation for transient periods, Figure 4 (a) shows the time derivative of $h_n(t)$ for the compressible and incompressible models. We see that up to degree 25, the deformation rates for the compressible model are larger for all time instants and the difference in the rates becomes smaller with time.

The relative increase in the rate is the largest for $n = 2$ (approximately 20% with respect to the incompressible case for t=1-3 kyrs) and gradually decreases with n. For $n \geq 35$, the rate for the compressible model is larger for short time scales and turns to be smaller for longer time scales. The relative difference after $t = 1$ kyrs is approximately 10% and does not change with n very much.

The above effects due to compressibility are inconsistent with the results of previous studies [Vermeersen et al., 1996; Hanyk et al., 1995]. This results from adopting the different definition for the incompressible model. When we employ the incompressible model with the same elastic rigidity as the compressible model, the deformation rate for $n = 2$ decreases by approximately 15% by considering compressibility (Figure 3 (b)), which is qualitatively consistent with the deceleration seen in Vermeersen et al. [1996], although the change is smaller than their result. The acceleration in the vertical displacement rate for higher degrees (Figure 3 (b)) is also consistent with Hanyk et al. [1995]'s finding.

5.2.2. Love number *l*

Figure 3 (c) displays the computed viscoelastic load Love numbers l_n^{cmp} and l_n^{inc} in the same manner. We see that larger offsets occur in the horizontal deformation over all time scales, compared to the vertical deformation. The signature of l_n at $t = 0.1$ kyr in the compressible case is positive for all degrees, corresponding to a compression in the vicinity of the load (and vice versa for the incompressible model). The relative differences in the horizontal deformation at $t = 0.1$ and 1,000 kyrs are larger for lower and higher degrees, which makes a contrast to the case for the vertical displacement where the difference between the compressible and incompressible models is the largest for $n = 70$.

Figure 4 (b) shows the time derivative of l_n for the compressible and incompressible models. In contrast to the vertical deformation rate, the horizontal deformation rate for lower degrees becomes slower for the compressible model. The relative decrease in the rate amounts to approximately 40 %, for example, around t =70 kyrs for $n = 2$ and $t = 5$ kyrs for $n = 35$. The relative difference in the rates is the largest at $n = 35$ and is smaller with lower and higher degrees.

For incompressible models, it already has been shown that effects of fine layering are larger on the horizontal motion than the vertical one [e.g. Vermeersen and Sabadini, 1997]. The above results indicate that effects due to compressibility are also larger on the horizontal motion than on the vertical motion for a multi-layer model including a lithosphere.

It is interesting to note that there is a negative correlation between the rate difference in the h Love number and that in the l Love number. In other words, when the difference in $\dot{h}$ is positive/negative, the difference in $\dot{l}$ is negative/positive (Figure 4 (d)). This indicates that considering compressibility generates differences in the surface deformation illustrated in Figure 5. The spatial variation similar to dilatation might imply that the condition of divergence free imposes a geometrical constraint on the deformation rate for the incompressible model, when compared to the compressible model. Identifying a plausible mechanism to explain this relationship, however, is very hard from surface deformation only. A comparison in the internal deformation and stress field will be needed to reveal it. The code used in this study cannot calculate internal deformation, since the numerical inverse Laplace integration in Eq. (2) must be carried out at each depth, which is computationally expensive. We will modify the code to compute the internal deformation more effectively.

5.2.3. Love number k

Figure 3 (d) displays the computed viscoelastic load Love numbers k in the same manner. We see that for $n \leq 10$, the effects enhance the total differences in the potential field between $t = 0.1$ and 1,000 kyrs. The relative differences to the incompressible case amount to 10% ($n = 2$) to 40% ($n = 4, 10$). For $n \geq 25$, the absolute values of k for the compressible model are always smaller than those for the incompressible model, and the relative offsets increase with n. Figures 4 (c) and (d) show the rates for k_n and the difference in the rates, respectively. The effect due to compressibility on $\dot{k}_n$ is similar to that on the vertical deformation (Figure 4 (a)). The relative rate difference is the largest for $n = 2$ (approximately 25% for t =1-5 kyrs), and decrease with n as in the case for the Love number h_n.

5.3. Effects on postglacial rebound models and sensitivity by GRACE

Wahr and Velicogna [2003] estimated present-day secular variations in the geoid due to postglacial rebound (PGR), using several plausible models based on the PREM and ICE3G [Tushingham and Peltier, 1991]. The secular variations predicted for these models were approximately 0.1 mm/yr for degrees $n < 30$ and their deviations caused by employing different viscosity profiles and elastic structures amount to approximately 10%. These differences in the lower-degree gravity potential coefficients were detectable with the GRACE (Gravity Recovery and Climate Experiment) satellites (Figure 1 of Wahr and Velicogna [2003]).

According to our computations in the previous section, the rate difference in the k Love number is 10-25% between the compressible and incompressible models for $n < 30$ and t =1-10 kyrs (Figure 4 (c)). We may consider roughly that these rate differences will produce differences of the same order of magnitude in the estimate of the present-day secular changes due to PGR, although the spatial distribution and time history of ice sheets are neglected in the Love number based on a point mass load. Effects due to compressibility are comparable to those caused by employing different earth model parameters, hence sensible by GRACE.

6. Conclusions

We have presented the validity of the method based on Tanaka et al. [2006, 2007] to compute surface loading of a radially symmetric self-gravitating viscoelastic earth model. This method does not modify the governing equations of Dahlen [1974] and Wu and Peltier [1982] for a compressible earth model and imposes no additional constraints on the density and viscoelastic profiles. We just carry out the numerical inverse Laplace integration along a rectangular path including all roots. The results computed with our method agree with those obtained by independent methods in both compressible and incompressible cases.

Using this method, we computed load Love numbers for an earth model based on the PREM and a convex viscosity profile. We compared our results with those for the incompressible material by setting not only the Poisson ratio to 0.5, but in addition we scaled the shear modulus to $0.5\mu_{cmp}/(1-\nu_{cmp})$. Also for this parameterization, we confirmed that major differences occur between the compressible and incompressible models. For the Love numbers h and k, the rate differences with respect to the incompressible case are the largest for lower harmonic degrees $n = 2 - 10$, which amount to increases of 10-25%. For the Love number l, the rate difference can amount to 40% for all degrees. The effects due to compressibility are in general larger on the horizontal deformation than on the vertical deformation. When the above parameterization is not employed, the effects due to compressibility on the Love numbers increase more, and their characteristics are consistent with previous results [Hanyk et al., 1995; Vermeersen et al., 1996].

We have not discussed mechanisms that cause the above differences. The presented method cannot separate the contributions from each normal mode or remove a root from the integration path as long as it is not an isolated root. Moreover, the present code cannot calculate internal deformation effectively. We will modify the code to calculate the radial profile of the deformation in a more efficient way to enable us to investigate the effects due to compressibility in more detail. The Fortran code used in this study will be implemented in the code for computations of co- and post-seismic deformation presented by Okuno et al. [2008] (this issue) in the near future. This method will contribute to increase accuracy for modeling postglacial rebound using compressible earth models through inter-comparisons with results obtained by other numerical approaches.

Acknowledgments. We acknowledge Bert Vermeersen and another anonymous reviewer for the insightful comments. We also acknowledge Detlef Wolf for the valuable comments on an earlier version of the manuscript. This work was carried out while YT was visiting GFZ, supported by a scholarship from the Ministry of Education, Culture, Sports, Science and Technology, Japan. The research by VK was supported by the priority program SPP 1257 of the German Research Foundation (DFG). We used the computer systems of the Earthquake Information Center of the Earthquake Research Institute, the University of Tokyo.

References

Boschi, L., J. Tromp and R. J. O'Connell (1999), On Maxwell singularities in postglacial rebound, *Geophys. J. Int., 136*, 492-498.

Bullen, K.E. (1975), The Earth's Density, Chapman and Hall, London. Cathles, L.M. The Viscosity of the Earth's Mantle, Princeton University Press, Princeton.

Dahlen, F. A. (1974), On the static deformation of an Earth model with a fluid core, *Geophys. J. R. Astr. Soc., 36*, 461-485.

Dziewonski, A. M. and A. Anderson (1981), Preliminary reference earth model, *Phys. Earth planet. Inter., 25,* 297-356.

Fang, M. and B. H. Hager (1994), A singularity free approch to postglacial rebound calculations, *Geophys. Res. Lett., 21,* 2131-2134.

Fang, M. and B. H. Hager (1995), The singularity mystery associated with a radially continuous Maxwell viscoelastic structure, *Geophys. J. Int., 123,* 849-865.

Han, D. and J. Wahr (1995), The viscoelastic relaxation of a realistically stratified earth, and a further analysis of postglacial rebound, *Geophys. J. Int., 120,* 287-311.

Hanyk, L., J. Moser, D. A. Yuen and C. Matyska (1995), Time-domain approch for the transient responses in stratified viscoelastic Earth models, *Geophys. Res. Lett., 22,* 1285-1288.

Hanyk, L., C. Matyska and D. A. Yuen (1999), Secular gravitational instability of a compressible viscoelastic sphere, *Geophys. Res. Lett., 26*, 557-560.

Klemann, V., Wu, P. and Wolf, D. (2003), Compressible viscoelasticity: stability of solutions for homogeneous plane-earth models, *Geophys. J. Int., 153*, 569-585.

Lambeck, K. and S. M. Nakiboglu (1980), Seamount loading and stress in the ocean lithosphere. *J. Geophys. Res.*, **85**, 6403-6418.

Martinec, Z. (2000), Spectral-finite element approach to three-dimensional viscoelastic relaxation in a spherical earth, *Geophys. J. Int., 142*, 117-141.

Martinec, Z., M. Thoma and D. Wolf (2001), Material versus local incompressibility and its influence on glacial-isostatic adjustment, *Geophys. J. Int., 144*, 136-156.

Okuno, J., Y. Tanaka and S. Okubo (2008), Comprehensive computer code VERGIL –a new tool for viscoelastic response of a multi-layered sphere to (internal) dislocations, *Pure and Applied Geophysics*, submitted.

Peltier, W. R. (1974), The impulse response of a Maxwell Earth, *Rev. Geophys. Space. Phys., 12,* 649-669.

Plag, H.P. and Jüttner, H.U. (1995), Rayleigh-Taylor instabilities of a selfgravitating Earth, *J. Geodyn., 20*, 267-288.

Press, W.H., S.A. Teukolsky, W.T. Vetterling, and B.P. Flannery (1992), *Numerical Recipes in FORTRAN 77: The Art of Scientific Computing*, 2nd ed., Vol. 2, 915 pp., Cambridge University Press, London.

Purcell, A. (1998), The significance of pre-stress advection and internal buoyancy in the flat-Earth formulation, in *Dynamics of the Ice Age Earth: a Modern Perspective*, edited by Wu, P., pp. 105-122, Trans. Tech. Publications, Hetikon.

Ricard, Y. and B. Wuming (1991), Inferring the viscosity and 3-D density structure of the mantle from geoid, topography and plate velocities, *Geophys. J. Int., 105*, 561-571.

Spada, G. and L. Boschi (2006), Using the Post-Widder formula to compute the Earth's viscoelastic Love numbers, *Geophys. J. Int., 166*, 309-321.

Steffen, H., G. Kaufmann and P. Wu (2006), Three-dimensional finite-element modeling of the glacial isostatic adjustment in Fennoscandia, *Earth and Planetary Science Lett., 250*, 358-375.

Tanaka, Y., J. Okuno and S. Okubo (2006), A new method for the computation of global viscoelastic post-seismic deformation in a realistic earth model (I) -vertical displacement and gravity variation, *Geophys. J. Int.*, 164, 273-289.

Tanaka, Y., J. Okuno and S. Okubo (2007), A new method for the computation of global viscoelastic post-seismic deformation in a realistic earth model (II) -horizontal displacement, *Geophys. J. Int.*, doi: 10.1111/j.1365-246X.2007.03486.x.

Tushingham, A.M. and W.R. Peltier (1991), *J. Geophys. Res.*, **96**, 4497-4523.

Turcotte, D. L. and G. Schubert (1982), *Geodynamics*, John Wiley and Sons, New York, 450 pp.

Vermeersen, L.L.A., R. Sabadini and G. Spada (1996), Compressible rotational deformation. *Geophys. J. Int., 126*, 735-761.

Vermeersen, L.L.A. and R. Sabadini (1997), A new class of stratified viscoelastic models by analytical techniques, *Geophys. J. Int., 129*, 531-570.

Vermeersen, L.L.A. and J. X. Mitrovica (2000), Gravitational stability of spherical self-gravitating relaxation models, *Geophys. J. Int., 142(2)*, 351-360.

Wahr, J. and I. Velicogna (2003), What Might GRACE Contribute to Studies of Post Glacial Rebound? *Space Science Reviews*, **108**, 319-330.

Wolf, D. (1985a), The normal modes of a layered, incompressible Maxwell half-space, *J. Geophys., 57*, 106-117.

Wolf, D. (1985b), The normal modes of a uniform, compressible Maxwell half-space, *J. Geophys., 56*, 100-105.

Wolf, D. (1997), *Gravitational Viscoelastodynamics for a Hydrostatic Planet, Series C, No. 452*, pp. 96, Verlag der Bayerischen Akademie der Wissenschaften, Munchen.

Wolf, D. and G. Kaufmann (2000), Effects due to compressional and compositional density stratification on load-induced Maxwell viscoelastic perturbations, *Geophys. J. Int., 140*, 51-62.

Wolf, D. and G., Li (2002), Compressible viscoelastic earth models based on Darwin's law, in *Ice Sheets, Sea Level and the Dynamic Earth*, edited by Mitrovica, J.X. and Vermeersen, L.L.A., pp. 275-292, American Geophysical Union, Washington.

Wu, P. and Z. Ni (1996), Some analytical solutions for the viscoelastic gravitational relaxation of a two-layer non-self-gravitating incompressible spherical earth. *Geophys.J.Int., 126*, 413-436.

Wu, P. and W. R. Peltier (1982), Viscous gravitational relaxation, *Geophys. J. R. Astr. Soc., 70,* 435-485.

Zhong, S., A. Paulson and J. Wahr (2003), Three-dimensional finite-element modelling of Earth's viscoelastic response: effects of lateral variations in lithospheric thickness. *Geophys. J. Int., 155*, 679-695.

Figure Captions.

Figure 1.

Comparisons of viscoelastic load Love numbers, $h_n(t)$, n represents the harmonic degree. **(top)** The white squares are values read from Fig. 3 in Hanyk et al. [1995] and the black ones display the result computed by our method for the same earth model. **(bottom)** The white squares are read from Figs. 11 and 12 in Spada and Boschi [2006] and the black ones show our result for the same earth model (their PREM L200 model).

Figure 2.

The viscosity profile employed for the mantle. The horizontal axis denotes the radial distance from the center of the Earth r. For $d = a - r$ in km, where a=6371, $\log_{10} \eta(r) = -6.08 \times 10^{-13} d^4 + 3.42 \times 10^{-9} d^3 - 6.50 \times 10^{-6} d^2 + 5.46 \times 10^{-3} d + 2.00 \times 10^1$ in Pa s holds. The number of the layers is approximately 2,000.

Figure 3.

(a) Effects due to compressibility on time series of viscoelastic load Love number h_n. The horizontal axis denotes time since Heaviside loading was applied. Black and white squares represent h_n for the compressible and incompressible models, respectively.

(b) As for (a) but for the incompressible model with the same elastic rigidity as the compressible model.

(c) As for (a) but for the load love number l_n.

(d) As for (a) but for the load love number k_n.

Figure 4.

(a) A comparison in the deformation rates of the load Love numbers h_n in Figure 3 (a). Black and white squares represent dh_n/dt for the compressible and incompressible models, respectively.

(b) As for (a) but for l_n in Figure 3 (c).

(c) As for (a) but for k_n in Figure 3 (d).

(d) The difference between the rates of the load Love numbers for the compressible and the incompressible models. The vertical axes denotes $-[(\dot{h}, \dot{l}, \dot{k})_n^{cmp} - (\dot{h}, \dot{l}, \dot{k})_n^{inc}]$, respectively. Positive values in the vertical axis indicate that the absolute displacement rates for the compressible model are larger.

Figure 5.

Differences in the surface deformation rates in the vicinity of the load, caused by considering compressibility. Δ denotes a difference with respect to the incompressible case. $\Delta\dot{h}_n \equiv \dot{h}_n^{cmp} - \dot{h}_n^{inc}$ and so forth.

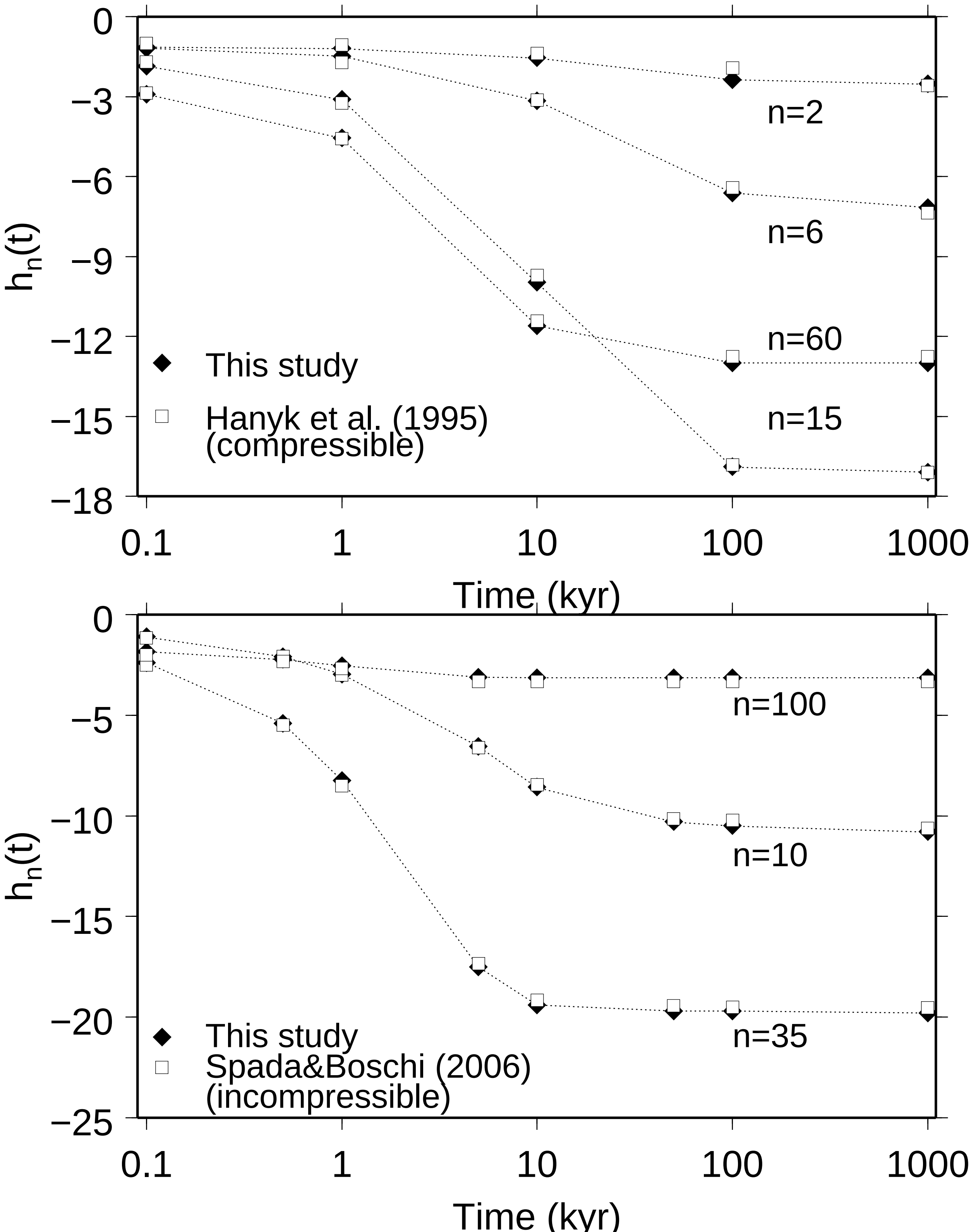

Figure 1. Comparisons of viscoelastic load Love numbers, $h_n(t)$, n represents the harmonic degree. **(top)** The white squares are values read from Fig. 3 in Hanyk et al. [1995] and the black ones display the result computed by our method for the same earth model. **(bottom)** The white squares are read from Figs. 11 and 12 in Spada and Boschi [2006] and the black ones show our result for the same earth model (their PREM L200 model).

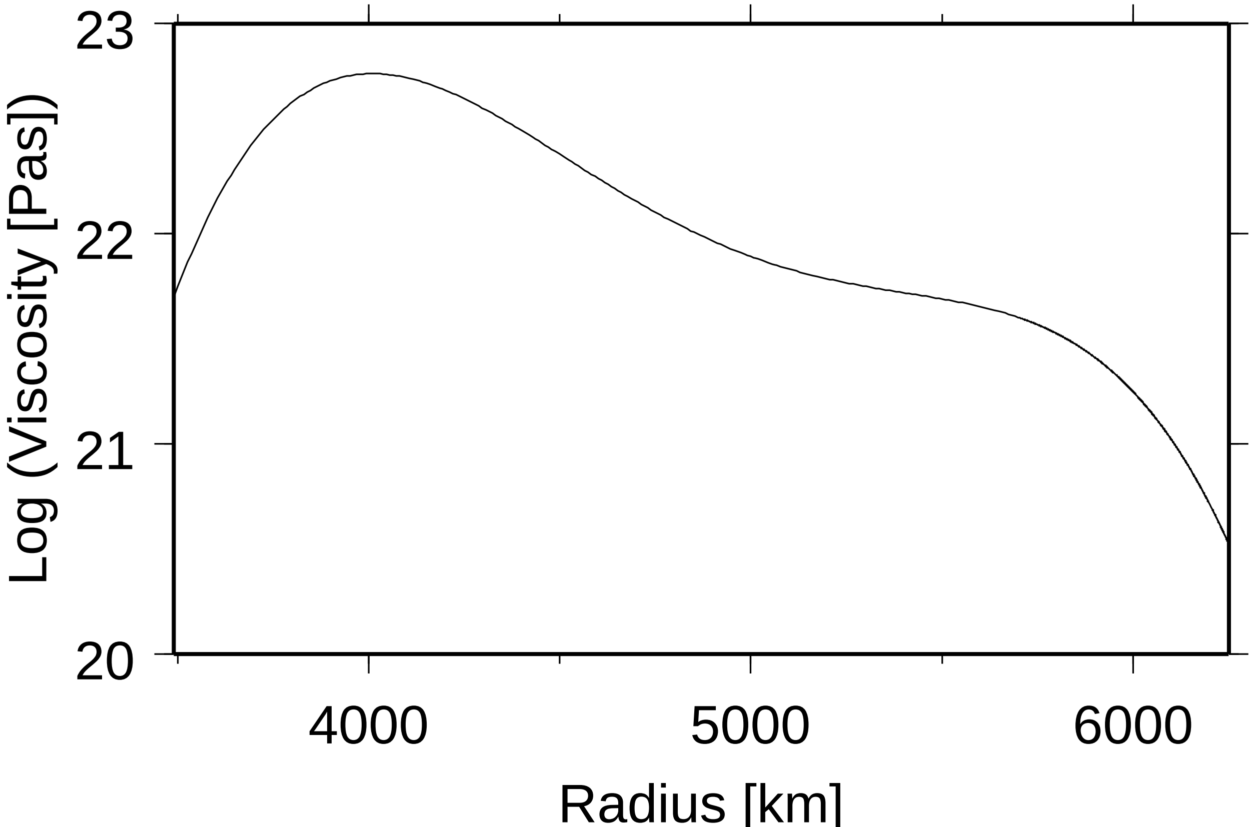

Figure 2. The viscosity profile employed for the mantle. The horizontal axis denotes the radial distance from the center of the Earth r. For $d = a - r$ in km, where a=6371, $\log_{10} \eta(r) = -6.08 \times 10^{-13} d^4 + 3.42 \times 10^{-9} d^3 - 6.50 \times 10^{-6} d^2 + 5.46 \times 10^{-3} d + 2.00 \times 10^1$ in Pa s holds. The number of the layers is approximately 2,000.

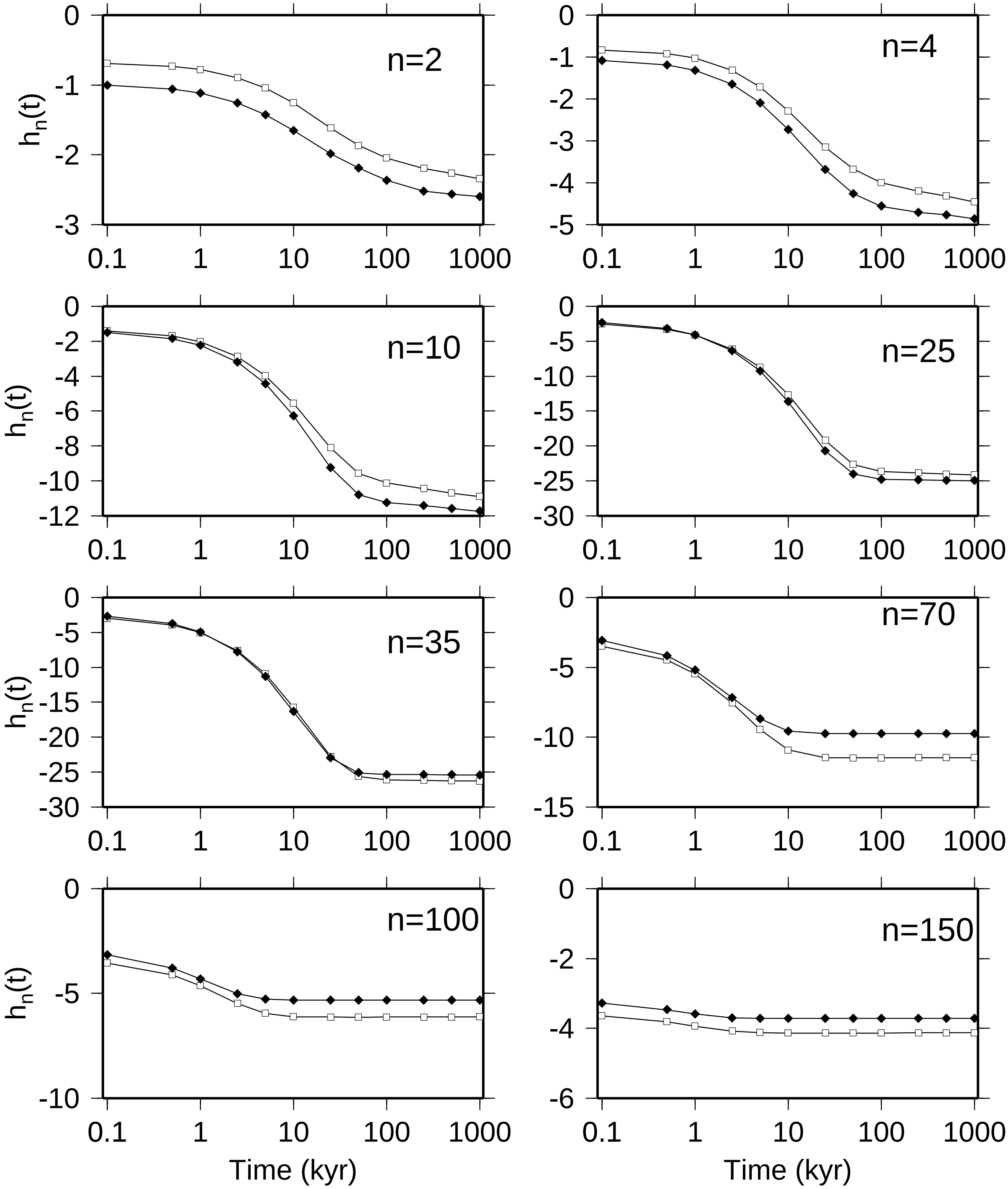

Figure 3 (a). Effects due to compressibility on time series of viscoelastic load Love number h_n. The horizontal axis denotes time since Heaviside loading was applied. Black and white squares represent h_n for the compressible and incompressible models, respectively.

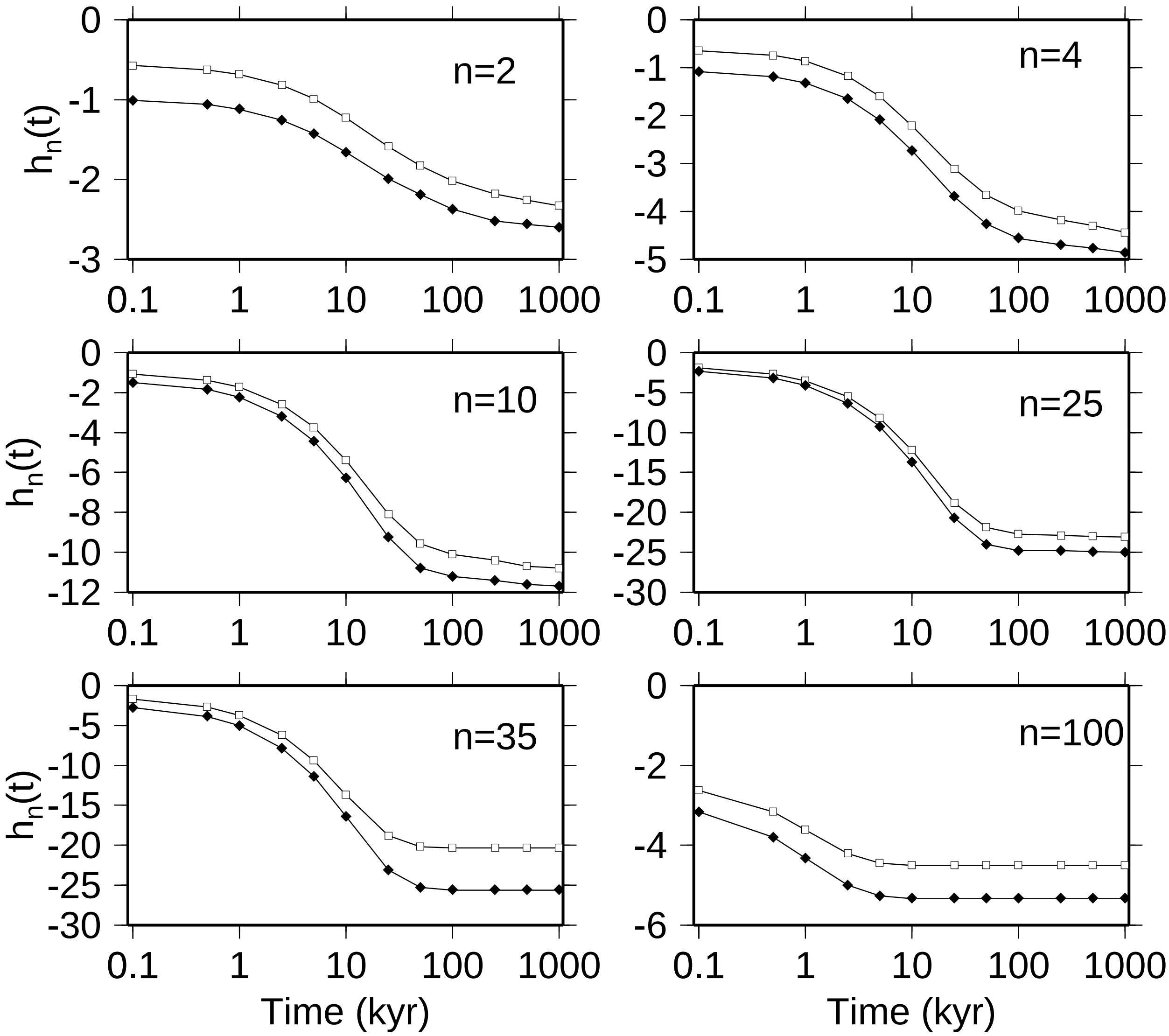

Figure 3 (b). As for (a) but for the incompressible model with the same elastic rigidity as the compressible model.

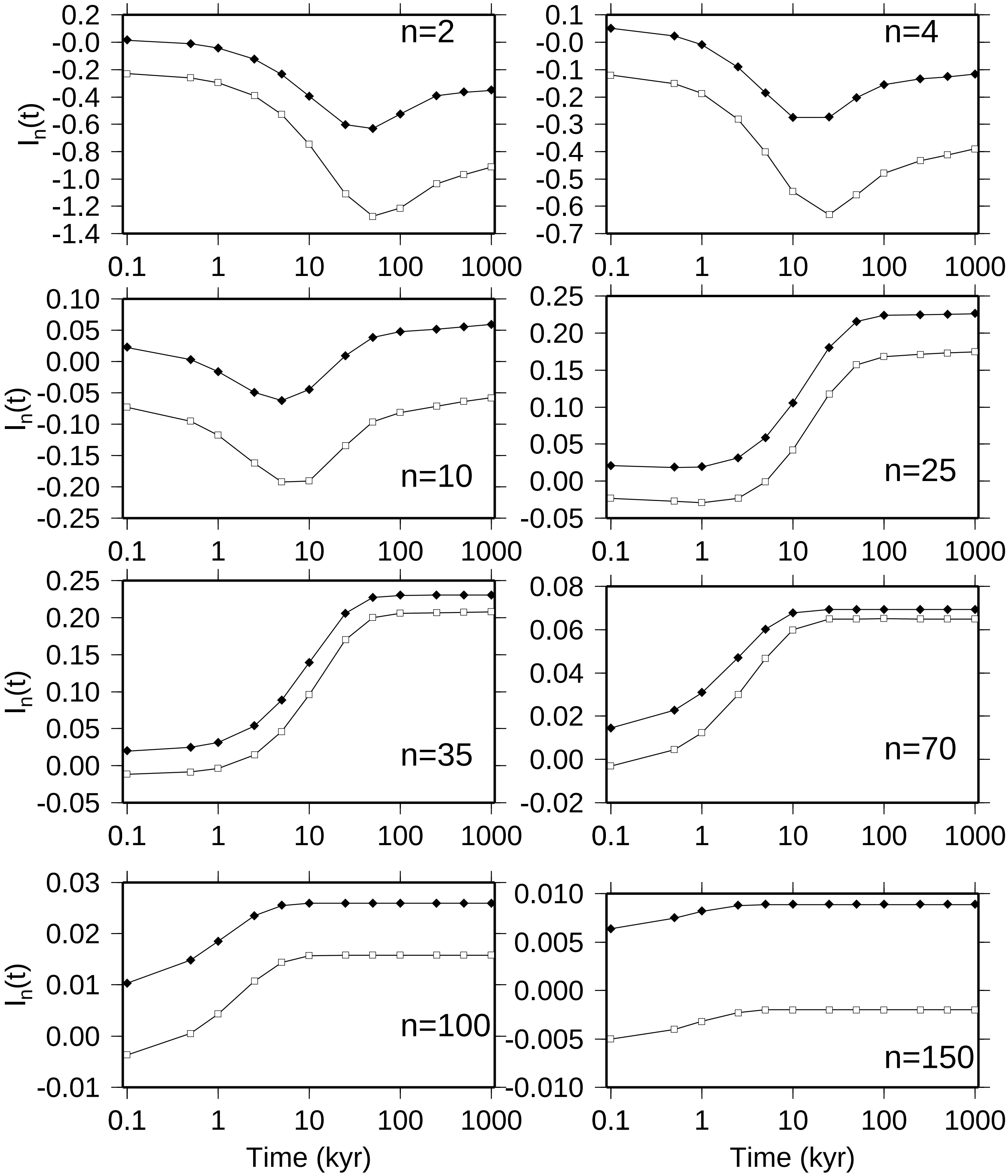

Figure 3 (c). As for (a) but for the load love number l_n.

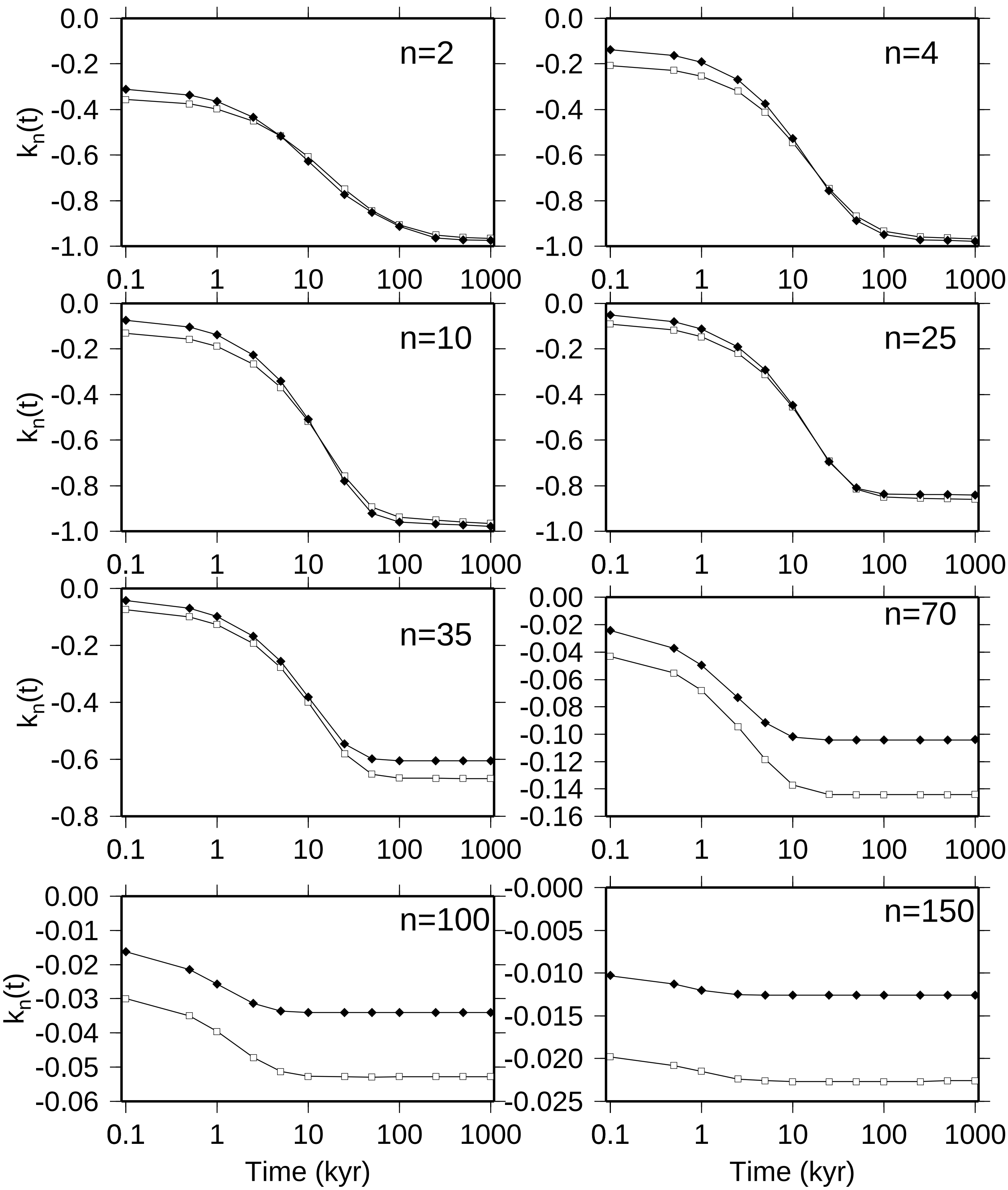

Figure 3 (d). As for (a) but for the load love number k_n.

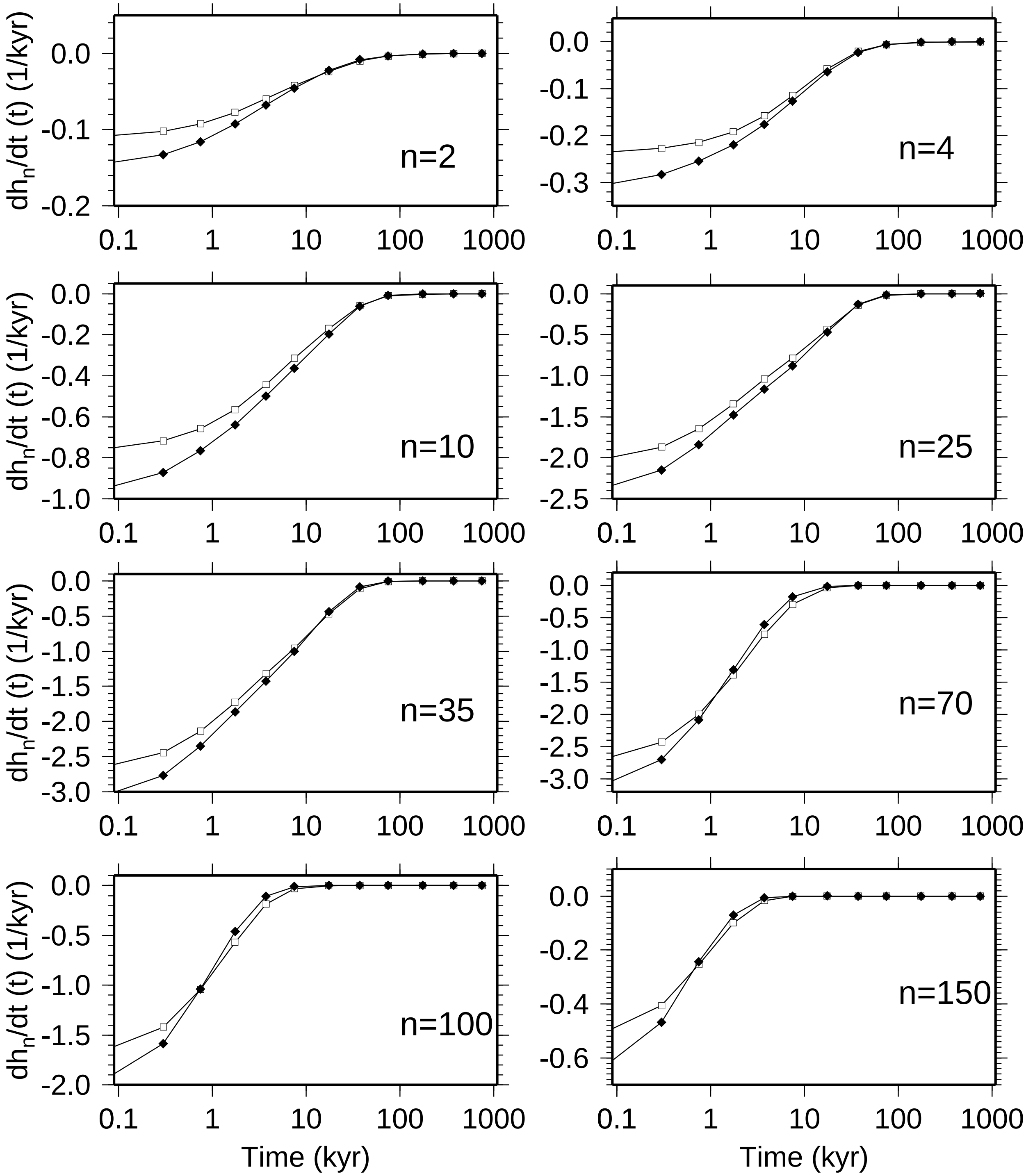

Figure 4 (a). A comparison in the deformation rates of the load Love numbers h_n in Figure 3 (a). Black and white squares represent dh_n/dt for the compressible and incompressible models, respectively.

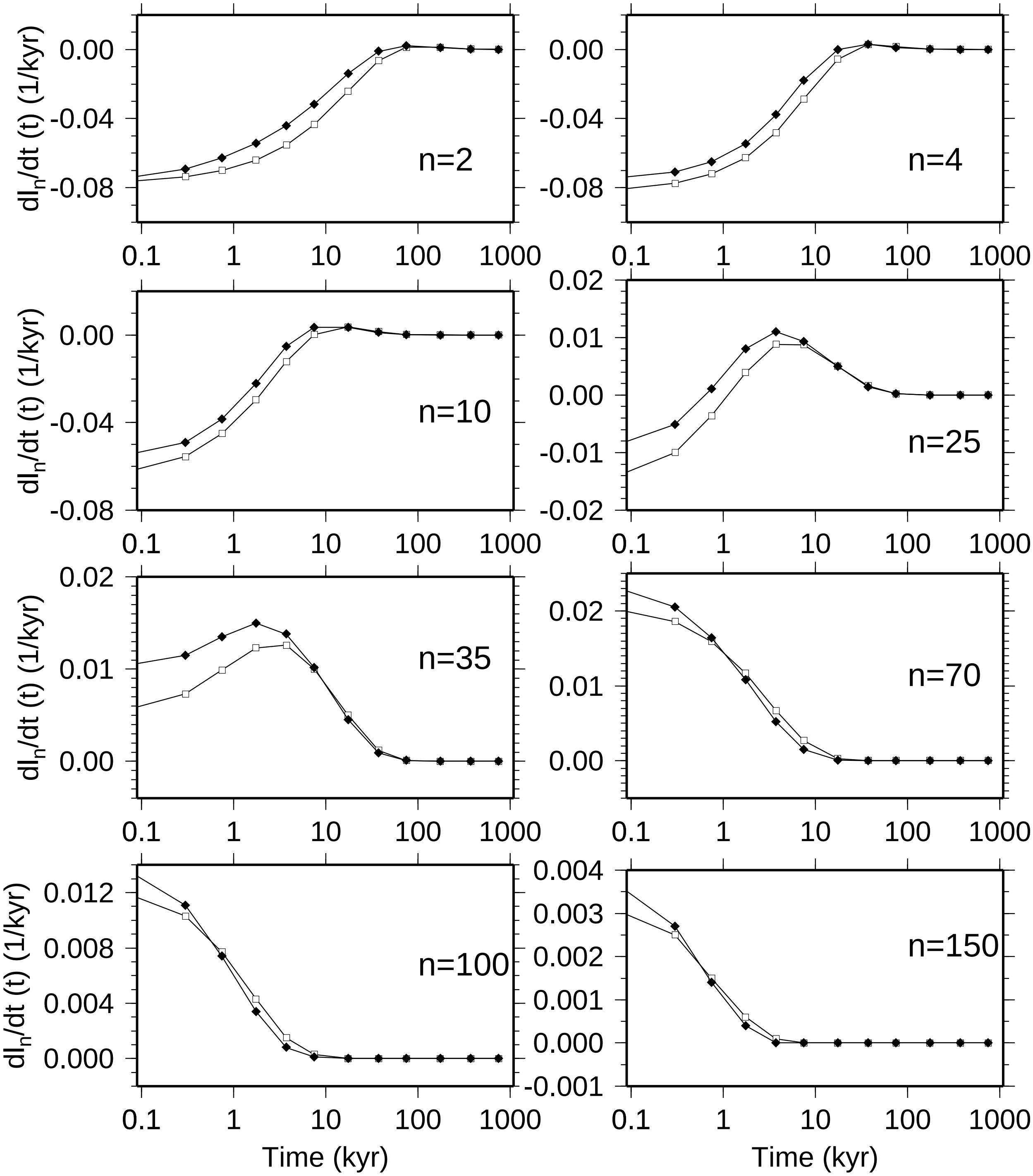

Figure 4 (b). As for (a) but for l_n in Figure 3 (c).

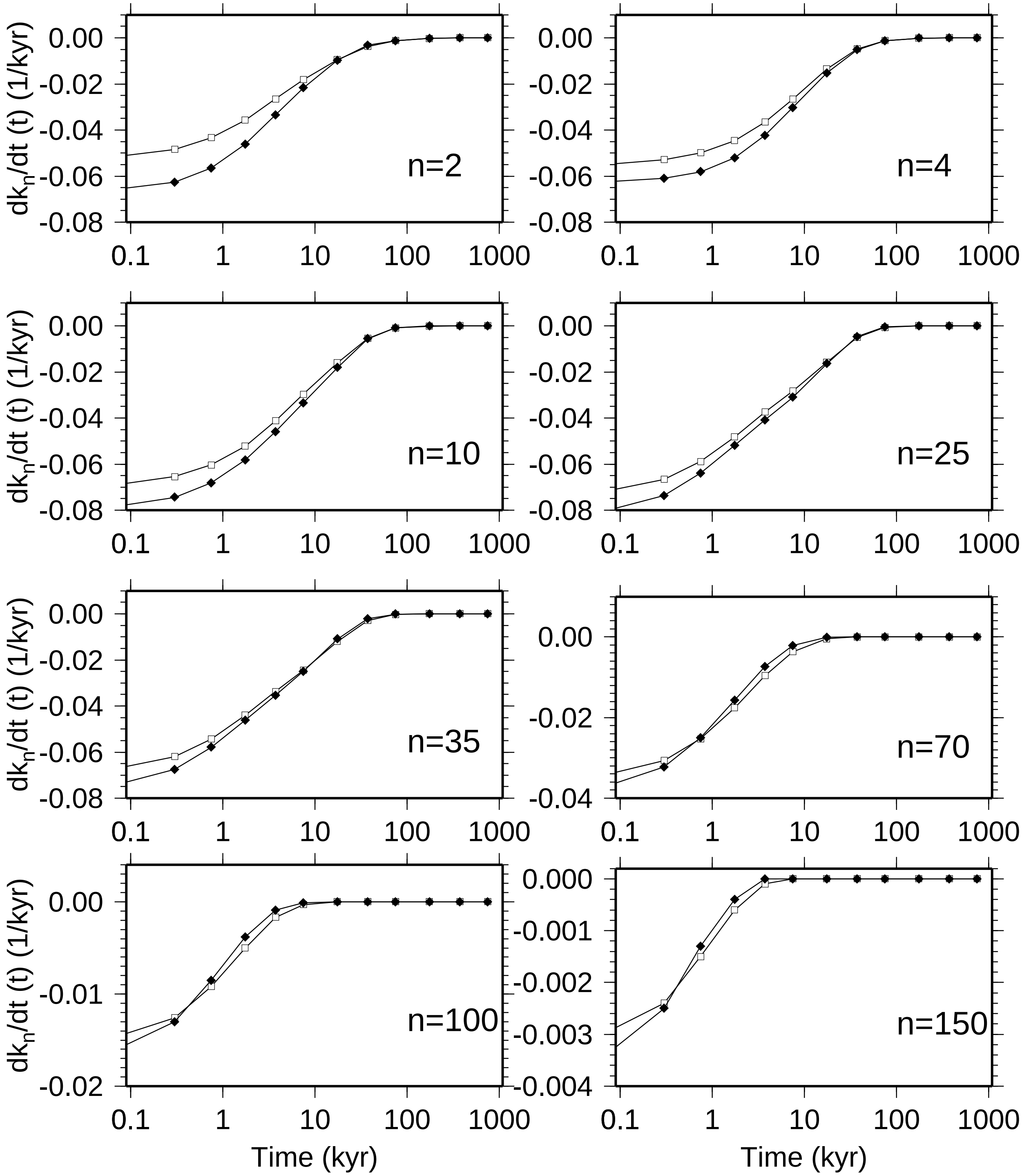

Figure 4 (c). As for (a) but for k_n in Figure 3 (d).

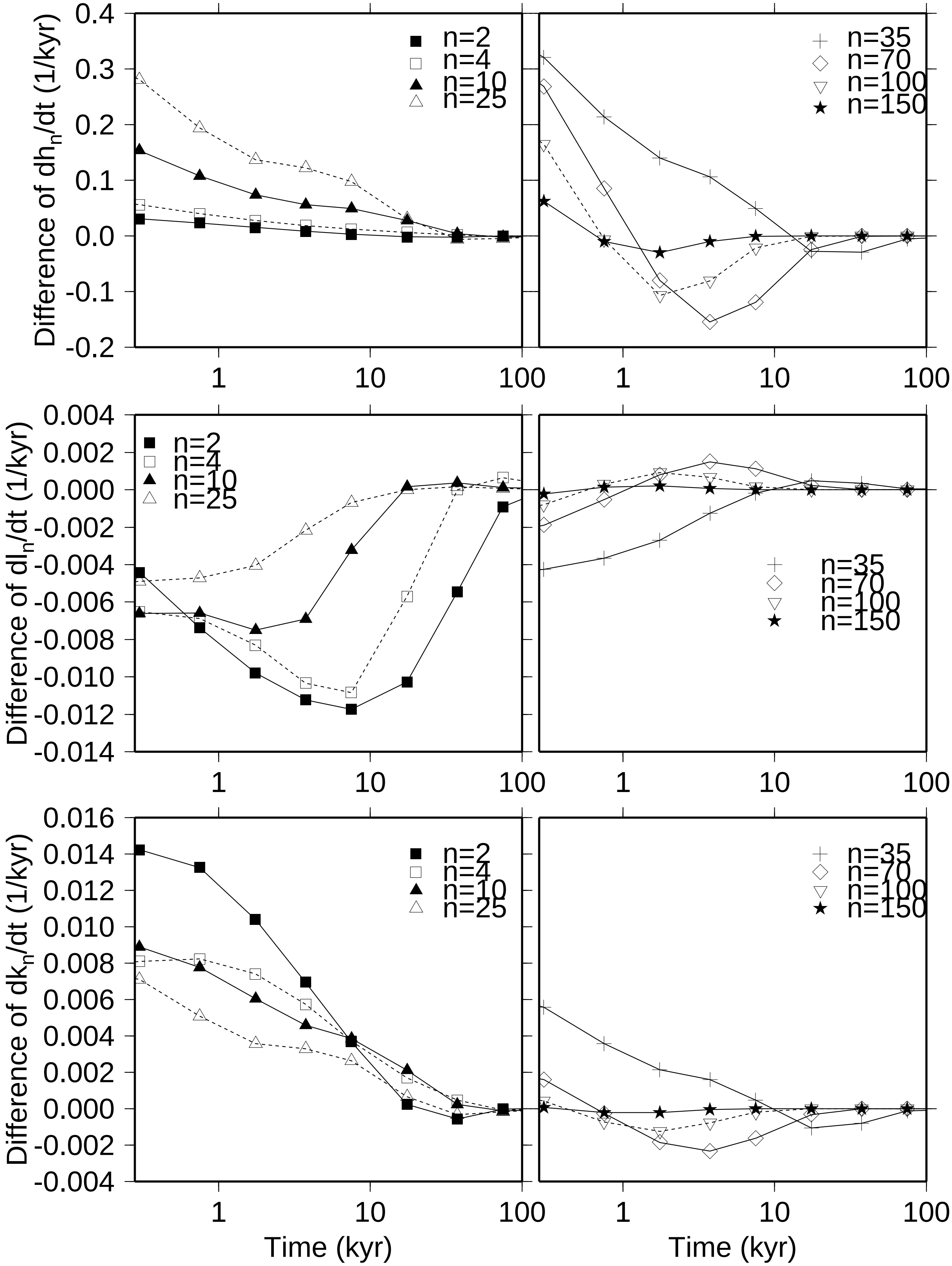

Figure 4 (d). The difference between the rates of the load Love numbers for the compressible and the incompressible models. The vertical axes denotes $-[(\dot{h}, \dot{l}, \dot{k})_n^{cmp} - (\dot{h}, \dot{l}, \dot{k})_n^{inc}]$, respectively. Positive values in the vertical axis indicate that the absolute displacement rates for the compressible model are larger.

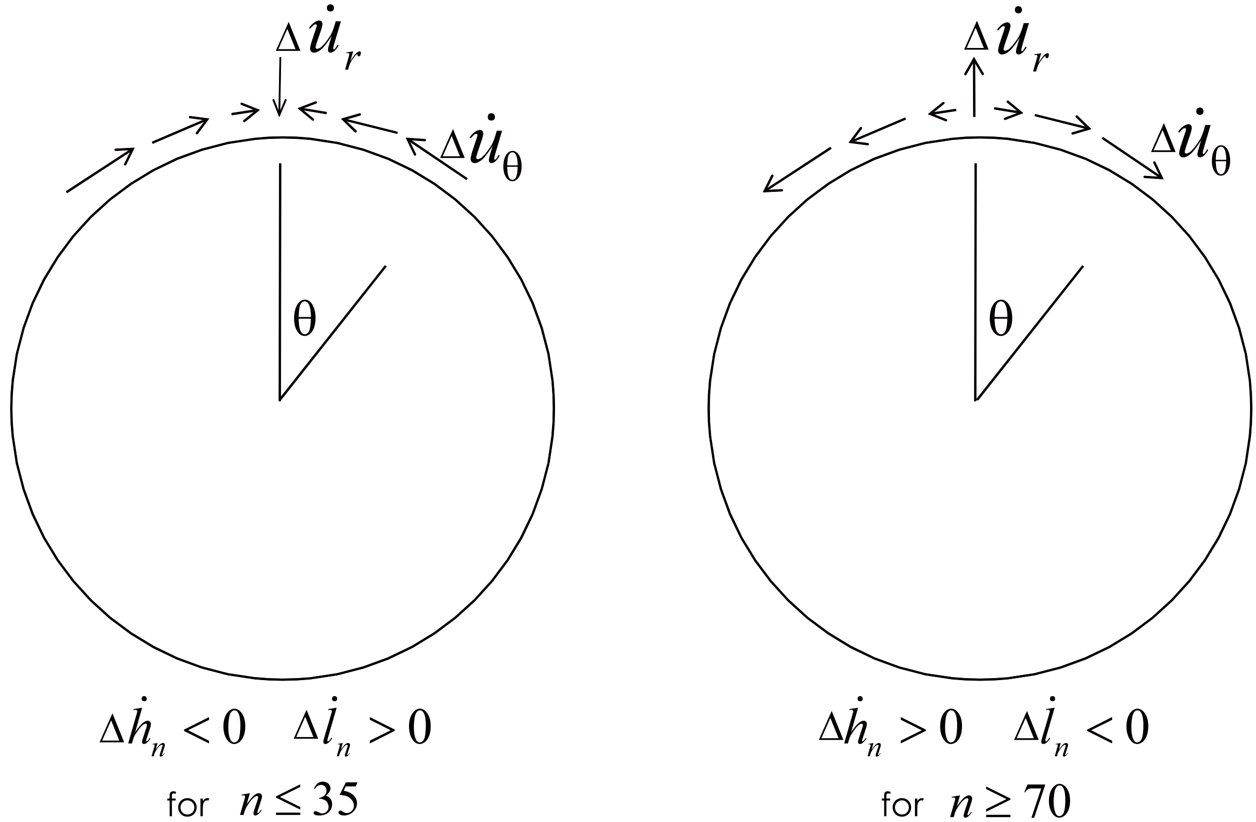

Figure 5. Differences in the surface displacement rates in the vicinity of the load, caused by considering compressibility. Δ denotes a difference with respect to the incompressible case. $\Delta\dot{h}_n \equiv \dot{h}_n^{cmp} - \dot{h}_n^{inc}$ and so forth.